Highly-active Pd–Cu electrocatalysts for oxidation of ubiquitous oxygenated fuels

Alexey Serov[a], Tristan Asset[b,c], Monica Padilla[a], Ivana Matanovic[a,1], Ulises Martinez[a], Aaron Roy[a], Kateryna Artyushkova[a], Marian Chatenet[b,c,d], Frederic Maillard[b,c], Domnik Bayer[e,2], Carsten Cremers[e], Plamen Atanassov[a,*]

[a] Department of Chemical & Biological Engineering and Center for Micro-Engineered Materials (CMEM), The University of New Mexico, Advanced Materials Laboratory, Albuquerque, NM 87131, USA
[b] University Grenoble Alpes LEPMI, F-38000 Grenoble, France
[c] CNRS, LEPMI, F-38000 Grenoble, France
[d] Institut Universitaire de France, Paris, France
[e] Fraunhofer Institute for Chemical Technology, ICT, Pfinztal, Germany

ABSTRACT

Nanostructured palladium-copper electrocatalysts with Pd:Cu ratios of 1:3, 1:1, and 3:1 were synthesized using a Sacrificial Support Method (SSM) in combination with the thermal reduction of metal precursors. The materials were comprehensively characterized by X-ray diffraction (XRD), X-ray Photoelectron Spectroscopy (XPS), Scanning and Transmission Electron Microscopy (SEM and TEM), surface area measurements (Brunauer-Emmett-Teller, BET) and Differential Electrochemical Mass Spectroscopy (DEMS). The SSM method enables the preparation of nano-sized unsupported Pd-Cu catalysts with uniformly-distributed particles and high surface area, in the range of $40 \, m^2 \, g_{catalyst}^{-1}$. Their catalytic activity for the electrooxidation of several alcohols (methanol, ethanol, ethylene glycol and glycerol) was investigated in alkaline media. In situ Infrared Reflection Adsorption Spectroscopy (IRRAS) and Density Functional Theory (DFT) calculations were used in order to understand the mechanism of the various alcohols electrooxidation reactions.

© 2016 Elsevier B.V. All rights reserved.

1. Introduction

Direct Liquid Fed Fuel Cells (DLFFCs) recently attracted attention of many researchers around the globe due to their multiple advantages, linked to the use of liquid fuels instead of hydrogen gas. Among these benefits, one can cite their high volumetric and gravimetric energy densities as well as the simplicity of storage, transportation and distribution of their fuel [1–3].

Alcohols are one example of liquid fuels that have been considered as promising for DLFFCs, since their use is compatible with broad applications, from mobile to back-up power devices. In addition, several alcohols are side-products of biomass conversion, which makes them "greener" than fuels of fossil origin, and they can

be valuable alternatives to hydrogen. The existing alcohol-fed DLF-FCs prototype devices operate with proton exchange membranes of the perfluorosufonic family, mainly Nafion®-based polymers. At the moment, such systems have lower performance compared to hydrogen-fed PEMFCs, due to detrimental fuel cross-over, slow kinetics of alcohol electrooxidation, and low stability and durability mainly because of their poisoning by side-products or intermediates of electrooxidation [1–3]. Furthermore, platinum which is the main catalyst used in DLFFCs is an expensive and rare metal hindering the wide deployment of this fuel cell technology. Therefore, electrocatalysts materials that could substitute platinum are currently explored extensively by the scientific community.

It is well known that palladium and palladium-based nanostructured materials have wide applications in the field of electrocatalysis for the fuel cells application [4]. Those materials can be utilized in Membrane Electrode Assembly (MEA) either on the cathode [4,5] or on the anode sides of DLFFC [6–12]. As stated by Antolini, the activity of Pd for alcohol oxidation is very low in acidic media but relatively high in alkaline media [4]. Additionally, the activity of Pd for alcohol oxidation can be enhanced by

adding a co-catalytic element, mainly metal (either d- or p-metals), or compounds such as oxides [4].

In that context, the present paper targets the substitution of platinum-based catalysts by cheaper materials based on palladium for the alkaline/anion exchange membrane fuel cell application with the utilization of several C_1–C_3 alcohols (methanol, ethanol, glycerol and ethylene glycol). This work also investigates the improvement of the activity of pure palladium by promotion effect using copper metal and oxides. The activity of unsupported palladium was compared to that of family of nanostructured Pd-Cu electrocatalysts (with the ratio between Pd and Cu: 1:3, 1:1 and 3:1) synthesized by the same method. The materials were prepared using the Sacrificial Support Method (SSM) [13–26], previously developed at UNM with a modification for the preparation of unsupported platinum group metals electrocatalysts. The SSM is a powerful and flexible method, which can be adopted for the synthesis of tailored high-surface area self-supported electrocatalysts and other classes of nanostructured materials. We are reporting that the above-mentioned materials can be considered as promising electrocatalysts for utilization in DLFFC anodes fed with C_1–C_3 oxygenated molecules.

2. Experimental

2.1. Catalyst preparation

High surface area silica (Cab-O-Sil^{TM} EH-5, surface area: $\sim$400 $m^2\,g^{-1}$) was firstly dispersed in water using a high energy ultrasonic probe. Appropriate amounts of $Pd(NO_3)_2 \times xH_2O$ and $Cu(NO_3)_2 \times xH_2O$ (Sigma-Aldrich) were added to the aqueous silica suspension. The overall metal loading on silica was targeted to *ca.* 25 wt% of final electrocatalyst after reduction. The silica and metal precursors' suspension was then allowed to dry on ultrasonic bath overnight. The obtained dry powder was ground in an agate mortar and pestle until a fine powder was obtained. It was then thermally reduced in 7% H_2 atmosphere (100 $cm^3\,min^{-1}$ flow rate) at T = 300 °C, for 2 h. After reduction, the catalysts were passivated in a flow of technical-grade nitrogen ($\sim$0.1 at.% O_2). The silica support was etched by means of 8 M KOH overnight and the resulting unsupported Pd_xCu_y electrocatalysts were washed with de-ionized water (DI water) until neutral pH was reached. The values of atomic Pd to Cu ratio were selected as 3:1, 1:1 and 1:3, and the corresponding electrocatalysts were nominally denoted as Pd_3Cu, $PdCu$ and $PdCu_3$, respectively. For comparison, unsupported palladium was also synthesized by the method described above (using the palladium nitrate only), and the catalytic activity of the Pd_xCu_y electrocatalysts was compared with that of pure Pd.

2.2. Characterization

The electrocatalyst materials were characterized is terms of morphology, phase composition, and chemical composition using SEM (Hitachi S-5200 Nano SEM, with an accelerating voltage of 15 keV), TEM (JEOL 2010, with an accelerating voltage of 200 keV), XRD and X-Ray Energy Dispersive Spectroscopy (X-EDS). SEM and TEM provided information on the morphology of the bulk and individual particles of the electrocatalysts while X-EDS was used to estimate the composition of the samples and compare it to the target composition. X-ray diffraction was performed using a Scintag Pad V diffractometer (Bragg-Brentano geometry) and DataScan 4 software (from MDI, Inc.) was utilized for system automation and data collection. Cu Kα radiation (40 kV, 35 mA) was used with a Bicron Scintillation detector (pyrolytic graphite curved crystal monochromator). Surface areas were also measured by nitrogen

sorption (Brunauer–Emmett–Teller method) using a Micromeritics 2360 Gemini Analyzer.

In situ Infrared Reflection-Adsorption Spectroscopy (IRRAS) experiments were performed at room temperature with a Nicolet 6700 FTIR spectrometer equipped with a liquid-nitrogen-cooled Mercury Cadmium Telluride (MCT) detector (see Refs. [27,28] for details of the setup). Each spectrum was obtained from 128 co-added spectra, acquired at a resolution of 8 cm^{-1}, using non-polarized light, during a slow-scan linear sweep voltammetry (scan rate at v = 0.001 V sec^{-1}). The data was presented in terms of absorbance of the spectra, defined as $A = -\log(R/R_0)$, where R and R_0 represent reflected IR intensities corresponding to the sample and reference single beam spectrum, respectively. In this configuration, a positive band in the spectrum signs the appearance of chemical species, while a negative band indicates a decrease in the concentration of a species (or disappearance), as compared to the reference spectrum. The reference spectrum was collected at E = −1.10 V vs. Ag/AgCl/Cl$^-_{sat}$. In all cases, the potentials have been corrected to the reversible hydrogen electrode (RHE) scale. The working electrode was prepared by depositing a thin layer of ink of the electrocatalyst onto a polished glassy carbon electrode with a diameter of 5 mm. The IR window was a ZnSe hemisphere, and the working electrode was gently pressed against this window, creating a thin solution layer with a thickness of a few micrometers. The incident angle of the IR radiation passing through the ZnSe window was 36°. During the whole experiment, argon was purged into the electrolyte, and the spectrometer and chamber were purged by dry air, reducing the spectral interference from ambient CO_2 and water vapor.

XPS spectra were acquired on a Kratos Axis DLD Ultra X-ray photoelectron spectrometer using a monochromatic Al Ka source operating at 150 W with no charge compensation. The base pressure was about 10^{-10} Torr, and operating pressure was 10^{-9} Torr. Survey and high-resolution spectra were acquired at pass energies of 80 and 20 eV respectively. Data analysis and quantification were performed using CasaXPS software. A linear background subtraction was used for quantification of C1s and O1s spectra while a Shirley background was applied to Cu2p and Pd3d spectra. Sensitivity factors provided by the manufacturer were utilized. A 70% Gaussian/30%Lorentzian line shape was used in the curve-fit of N1s.

The electrochemical analysis of the synthesized material was performed by rotating disk electrode (RRDE) experiments using the Pine Instrument Company electrochemical analysis system. The revolution rate was set at Ω = 1600 RPM, and the scan rate at v = 0.020 V s^{-1}. The electrolyte was 1 M KOH containing 1 M of the studied alcohols (MeOH and EtOH) or 0.1 M in the case of EG and glycerol saturated in N_2 at room temperature. A platinum wire counter-electrode and Hg/HgO reference electrode were used, but the potentials were corrected for the RHE scale. The inks for working electrodes were prepared by mixing 5 mg of the desired Pd_xCu_y electrocatalyst with 925 μL of a water and isopropyl alcohol (4:1) mixture, and 75 μL of Nafion® (0.5 wt.%, DuPont). The mixture was mixed and dispersed by sonication, before 10 μL was applied onto a glassy carbon disk (surface area of 0.2472 cm^2). The loading of catalyst on the electrode was in all cases 0.2 $mg_{catalyst}\,cm^{-2}$.

DEMS measurements were performed in a flow thorough DEMS cell set-up. In this cell the working electrode consists of a thin micro-porous PTFE membrane provided by W.C. Gore. The membrane is sputter coated with a thin layer of gold so that most of the pores remain open. The gold is used as electron conductor for the catalyst layer which is applied by spray coating. The ink for the spray coating consist of 100 mg of catalyst dispersed in 3 g of ethanol to which 100 mg of Teflon® dispersion (DuPont) 5 wt% in water were added. As counter electrode, a platinum mesh placed in a separate compartment downstream of the working electrode compartment is used. As reference electrode, a Hg/HgO electrode is used, which is placed in a third compartment connected to the
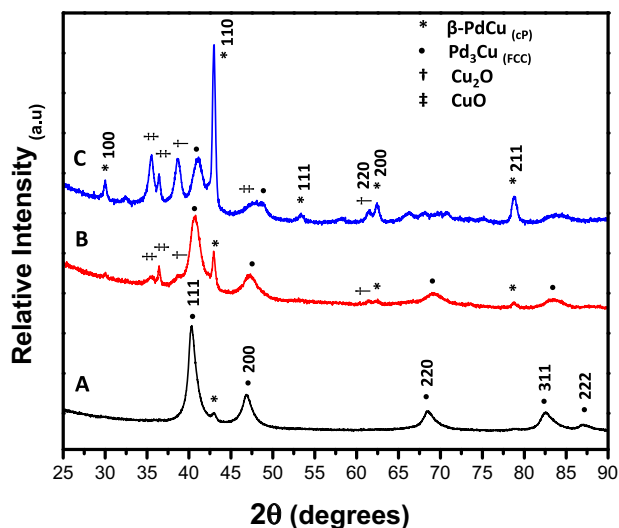
Fig. 1. XRD data for Pd-Cu catalysts: (A) Pd$_3$Cu, (B) PdCu, and (C) PdCu$_3$ prepared by Sacrificial Support Method.

working electrode compartment by capillary tubing through which a trickling stream of pure electrolyte is maintained. Mass spectrometric voltammograms (MSCVs) are recorded using a Gamry Reference 3000 potentiostat which receives the signals from the Balzer QMS 200 mass spectrometer as an additional analog input.

3. Results and discussion

The phase composition of the synthesized Pd$_x$Cu$_y$ materials was obtained from X-ray diffraction (XRD, Fig. 1). All the copper-containing samples consist of two palladium-copper phases: a face-centered cubic (FCC) solid solution and the primitive cubic phase β-PdCu. Additional phases, Cu$_2$O and CuO, were detected in samples with increased amounts of Cu (PdCu and PdCu$_3$). The total mass fraction of Cu oxides was calculated by XRD pattern refinement and was found to be 30 wt.% and 57 wt.% for PdCu and PdCu$_3$, respectively. In the case of the PdCu$_3$ catalyst (Fig. 1 (c)), equal amounts of the FCC and primitive cubic phase were observed with a mass fraction of 21 wt.%. However, increasing the concentration of Pd resulted in an increased amount of the FCC solid solution, becoming 61 wt.% and 97 wt.% for the PdCu and Pd$_3$Cu catalysts, respectively. Additionally, the lattice parameter (a) of the FCC solid solution phase was found to increase by *ca.* 1.0% at each incremental increase in Pd content: $a = 3.7973$, 3.8363 and 3.8782 Å for PdCu$_3$, PdCu and Pd$_3$Cu, respectively. This result is consistent with the gradual enrichment of the solid solution phase with palladium. The average size of crystallite domains was calculated using Scherrer equation for the Pd-Cu phases. For the FCC phase, the average domain sizes for the PdCu$_3$, PdCu and Pd$_3$Cu catalysts were of $d_{FCC} = 7$, 6 and 10 nm, respectively. For the primitive cubic phase, the average domain sizes were also roughly similar: $d_C = 21$, 20 and 18 nm for the PdCu$_3$, PdCu and Pd$_3$Cu catalysts, respectively.

The morphological analysis of the Pd$_x$Cu$_y$ catalysts was performed by SEM imaging. Fig. 2 (a–c) demonstrates that all materials have similar 3-D structures; the voids between the agglomerated particles resulted from the removal of the sacrificial support particles (~30 nm for fumed silica). The (less-abundant) presence of larger voids in the material originates from the existence of SiO$_2$ agglomerates within the colloidal silica, with a size of *ca.* 100 nm. Independent on overall composition, the prepared Pd$_x$Cu$_y$ catalysts displayed BET surface areas of *ca.* 40 m^2 g$_{catalyst}$$^{-1}$, which is noticeably large for unsupported catalysts. The TEM micrographs of palladium-copper materials (Fig. 3 (d–f)) demonstrate the fine dis-

tribution of the PdCu and Pd$_3$Cu nanoparticles in the form of open agglomerates; these agglomerates do not display signs of excessive coalescence (in other words, the crystallites touch each-other but remain separated in terms of crystalline lattice, which is in agreement with the small sizes of the crystallite domains d_C and d_{FCC} obtained by XRD). The picture drastically changes in the case of PdCu$_3$: the agglomerated nanoparticles coalesce into larger features, which is likely due to the large copper concentration and Cu$_2$O oxide detected in XRD (indeed, the values of d_C and d_{FCC} are not significantly larger than for the PdCu and Pd$_3$Cu samples). For all materials the morphology of the Pd$_x$Cu$_y$ electrocatalysts is characterized by well-developed 3D structure, with large BET surface area and fine particle size distribution, thereby demonstrating the benefits of the Sacrificial Support Method.

High-resolution X-ray photoelectron spectroscopy was utilized to study the surface chemical composition of Pd$_x$Cu$_y$ electrocatalysts. The Pd/Cu ratios obtained for electrocatalysts were 1:3, 0.75:1, and 1.53:1 for PdCu$_3$, PdCu and Pd$_3$Cu, respectively. Surface segregation of Cu was observed, particularly for 1:1 and 3:1 samples. It should be noticed that sampling depth for Cu atoms is twice smaller than that for Pd, so particles with Cu shell around the Pd-Cu intermixed alloy, have an enrichment of Cu at the surface.

In order to obtain the surface composition of copper oxide a high-resolution Cu 2p spectrum was fitted with 4 peaks which were originated from: PdCu alloy phase at *931.6*eV; Cu$_2$O at *933.1*eV; CuO at *934.4*eV; and copper hydroxides at *936.1*eV. The substantially pronounced satellite peak which is indicative of copper oxide presence was also detected at higher binding energy. For Cu-rich sample PdCu$_3$, a large amount of higher binding energy (BE) peak from the copper oxides was observed with a palladium-copper phase peak being smallest (11.2 relative percent of the total copper presented in the samples). It was shown that for the samples with the highest nominal concertation of palladium in the materials, i.e. PdCu and Pd$_3$Cu, the relative intensity of palladium-copper phase peak increased up to 26 at.% for Pd$_3$Cu, which is direct indication of higher concentration of palladium atoms in the surface of electrocatalysts.

Further analysis included the fitting of high-resolution Pd 3d spectrum with 4 peaks that are coming from PdCu phase at *335.1–335.9*eV, PdO at *336.9*eV and PdO$_2$ at *338.1*eV. It was observed that the increase of Pd to Cu ratio in the electrocatalyst resulted in significant increase of the peak *335.1*eV intensity from 25% to 43%, while the peak at *335.9*eV stays the same. This observation was in good agreement with two categories of palladium-copper phase observed in XRD data (FCC and primitive cubic PdCu), so peak at *335.1*eV may be assigned to FCC while peak at *335.9* originates from primitive cubic palladium-copper phases.

The electrochemical data for oxidation of various light alcohols on the Pd$_x$Cu$_y$ electrocatalysts is summarized in Fig. 4, Fig. S1 and Table 1. Mass current densities were normalized to the mass of palladium, the most expensive element while kinetic limitations and onset of alcohol oxidation were evaluated using standard electrochemical criteria of current density. To allow for alcohol oxidation currents being registered at lower potentials than the onset itself, the onset potentials were defined as the value where the current density is equal to 5% of the peak current density, enabling the study of the influence of kinetic and Tafel slopes limitations at these potentials. The Tafel slopes *(b)* values were therefore given in a dual manner in Table 1: the *"below onset potentials"* Tafel slopes and *"above onset potentials"* Tafel slopes. In the case of some catalyst/alcohol combinations, further calculation of a relevant Tafel slope was impossible (gray numbers in Table 1). In all synthesized Pd-Cu catalysts, the addition of copper improves the electrocatalytic activity of Pd-Cu materials in comparison with pure metallic palladium. This is confirmed for all PdCu and Pd$_3$Cu catalysts and all four fuels. For the PdCu$_3$ on the other hand, the improvement
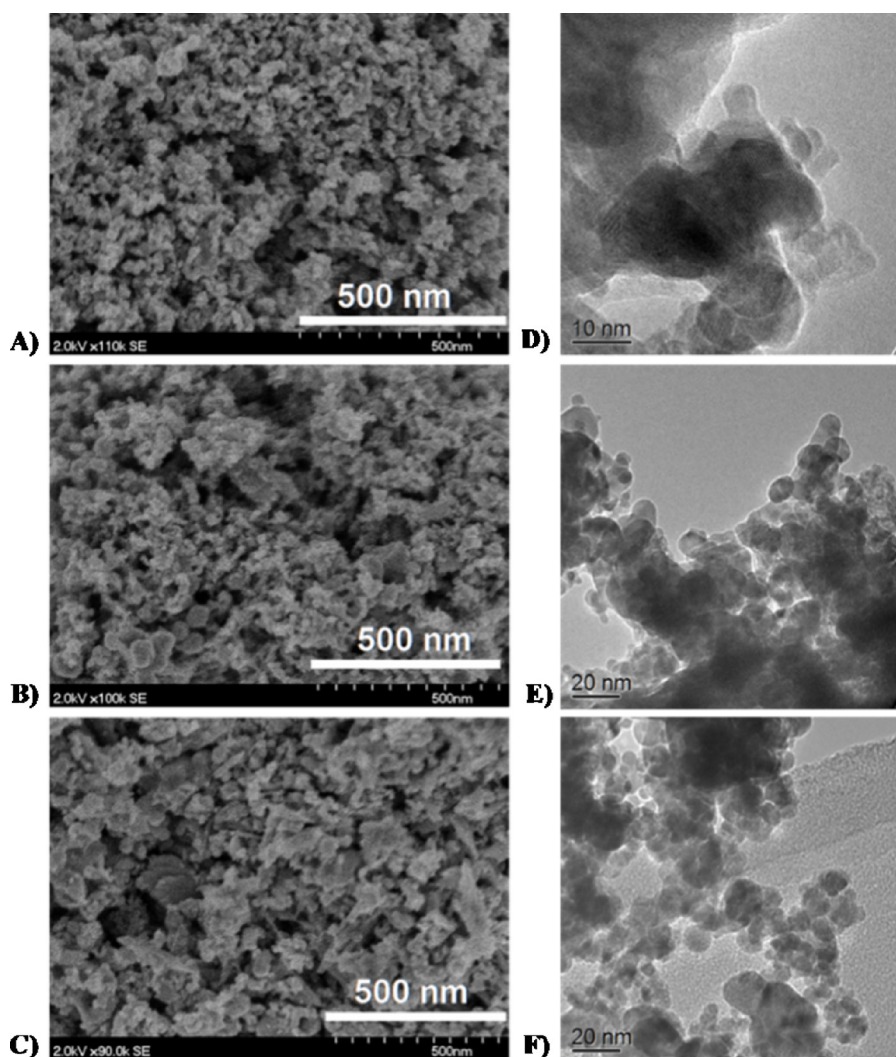
Fig. 2. SEM (A–C) and TEM (D–F) images for Pd_xCu_y catalysts prepared by thermal reduction of precursors. A, D: $PdCu_3$, B, E: PdCu and C, F: Pd_3Cu.

Table 1
Alcohol oxidation (MOR, EOR, EGOR and GOR) parameters for Pd_xCu_y and Pd catalysts. Tafel slopes (b) observed below the onset potential are given on the column left side, whereas the one observed above this potential are given right side. The absence of relevant Tafel slope was indicated by a grey marker in the table.

		Pd		Pd_3Cu		PdCu		$PdCu_3$	
Methanol	I ($A\,g_{Pd}^{-1}$) at **0.75 V** *vs*. RHE	85		**140**		110		55	
	Onset (V *vs*. RHE)	0.55		**0.5**		0.61		0.63	
	Tafel Slope (mV dec^{-1})								
Ethanol	I ($A\,g_{Pd}^{-1}$) at **0.75 V** vs. RHE	305		350		**435**		230	
	Onset (V *vs*. RHE)	**0.46**		**0.46**		**0.46**		**0.46**	
	Tafel Slope (mV dec^{-1})	**180**		195		210		160	230
Ethylene Glycol	I ($A\,g_{Pd}^{-1}$) at **0.75 V** *vs*. RHE	105		160		**200**		165	
	Onset (V *vs*. RHE)	**0.63**		**0.63**		**0.63**		**0.63**	
	Tafel Slope (mV dec^{-1})	205		150	175	200	170	200	**140**
Glycerol	I ($A\,g_{Pd}^{-1}$) at. **0.75 V** *vs*. RHE	75		65		**205**		105	
	Onset (V *vs*. RHE)	0.63		0.62		0.6		**0.59**	
	Tafel Slope (mV dec^{-1})		185		185			140	

was observed in the case of EG. As can be seen from Fig. 3A, Pd_3Cu was found to be the most active among the studied electrocatalysts towards the oxidation of methanol, followed by Pd and PdCu with the observed currents for Pd_3Cu and Pd being $140\,A\,g_{Pd}^{-1}$ *vs*. $85\,A\,g_{Pd}^{-1}$ (Table 1). In the case of ethylene glycol, all the Pd_xCu_y electrocatalysts exhibit increased performance *vs*. pure Pd. The electrocatalyst with the largest Cu-content $PdCu_3$ had a mass activity of of $165\,A\,g_{Pd}^{-1}$ in comparison to $105\,A\,g_{Pd}^{-1}$ for Pd (presented at 0.75 V *vs*. RHE (Fig. 4C and Table 1). Such behavior can

be explained by the synergy of the catalytic contribution of Cu_2O for ethylene glycol oxidation and intrinsic activity of the Pd_xCu_y phases.

The contribution of copper and copper oxides to the electrooxidation of alcohols in alkaline media, especially in the rate determining step, may occur by three different mechanisms: electronic [29–32], steric [33–35] and bi-functional effect [36–40]. In general, electronic effect occurs in the case of strong influence of add-atom on the electronic structure of main catalytic element;
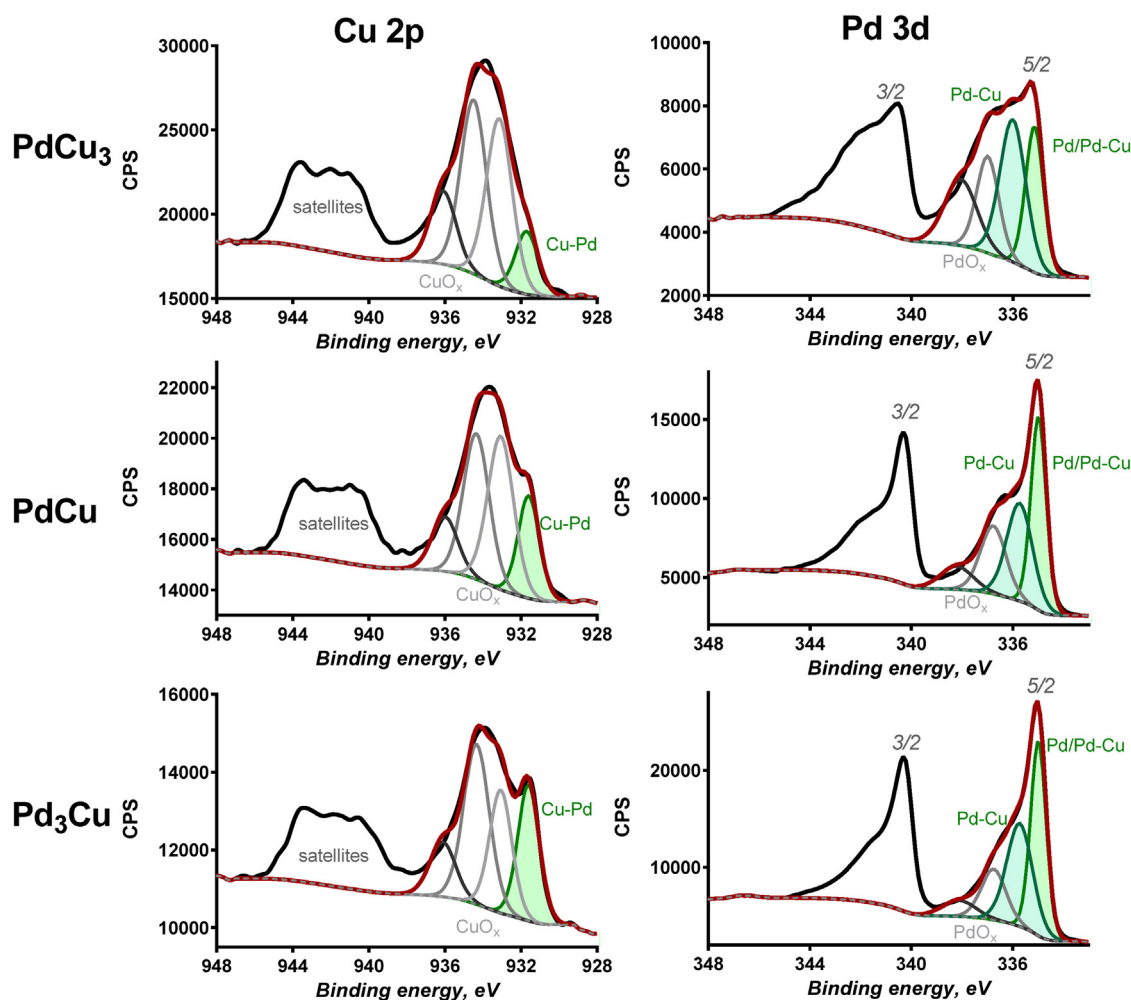
Fig. 3. High resolution XPS spectra of $PdCu_3$, $PdCu$ and Pd_3Cu electrocatalyst.

steric effect happens when add-atoms embed in the surface lattice of a catalyst in such a way that some active sites lose accessibility of intermediate products; and the bi-functional mechanism occurs in the case in which add-atom is as catalytically active towards the same type of reactions as a main active atomic site. Copper itself is not catalytically active in reactions of electrooxidation of oxygenated molecules, however, Cu, Cu_2O and CuO are well-known oxophilic element and compounds. Recently, an intrinsic effect of the alloying of the primary catalyst with a second metal resulted in a modification of the electronic structure leading to a higher catalytic performance. Oxophilic metals, such as Ru, Sn, and Ni, have shown to improve the catalytic performance of Pt and Pd catalysts for alcohol electrooxidation [41–45]. Taking into account high oxophilicity of copper and copper oxides, the adsorption of hydroxyls will be preferable in comparison to the noble surface of palladium. Ethylene glycol and glycerol may adsorb on the catalytic surface via more than one R—OH groups, and the rate of oxidation of those molecules will be directly dependent on the availability of hydroxyls in the vicinity of adsorbed —COH groups. Therefore, having copper and copper oxide populated with —OH groups will facilitate two step electrooxidation mechanism: (a) adsorption of EG and glycerol on the catalyst surface and (b) desorption of oxidized acyls [46].

Further electrochemical performance analysis revealed that the Tafel slope of $150 \, mV \, dec^{-1}$ was observed in the case of $PdCu_3$, compared to $205 \, mV \, dec^{-1}$ slope for Pd, followed by $200 \, mV \, dec^{-1}$ slope for PdCu and $PdCu_3$. It, therefore, appears that the catalytic

improvement is induced by copper or its oxides/hydroxides as well as by the FCC solid solution (below 0.6 V *vs.* RHE). The activity at potentials above 0.6 V *vs.* RHE revealed that $PdCu_3$ is characterized by the highest kinetics (Tafel slope of $140 \, mV \, dec^{-1}$), followed by PdCu and Pd_3Cu, with Tafel slopes of 170 and $175 \, mV \, dec^{-1}$, respectively. Such trend correlates with the increase of FCC PdCu solid solution content from $PdCu_3$ to Pd_3Cu and the amounts of Cu_2O—30 wt.% in PdCu and 57 wt.% in $PdCu_3$. PdCu outperforms all the other electrocatalysts for the oxidation of glycerol (Fig. 4D), whereas similar performances were observed for the EOR, *i.e.* after normalization by the catalyst total mass (Fig. S1 B). Finally, it is should be noted, that despite the fact that adding copper strongly affects the direct scan (Fig. 4), it does not significantly modify the voltamperometric features of the reverse scan reactivation peak, which is attributed to the reduction of the palladium surface oxides [3]. This peak develops at similar potential values (*ca.* 0.75 V *vs.* RHE) for nearly all catalysts and fuels, suggesting that copper adjunction to palladium does not have any significant influence on the desorption potential of OH_{ads} from Pd atoms (which was confirmed by further DFT calculation, see below).

$PdCu_3$, which contains a significant proportion of copper-oxide phases (57 wt%, including Cu_2O), shows an extremely low performance for methanol and ethanol oxidation, but a higher performance than Pd_3Cu and Pd electrocatalysts for the oxidation of ethylene glycol and glycerol (Table 1). Such an effect is based on promotion mechanism of oxides conjugated with decreased electrical conductivity of cuprous oxide. Much larger peak currents are
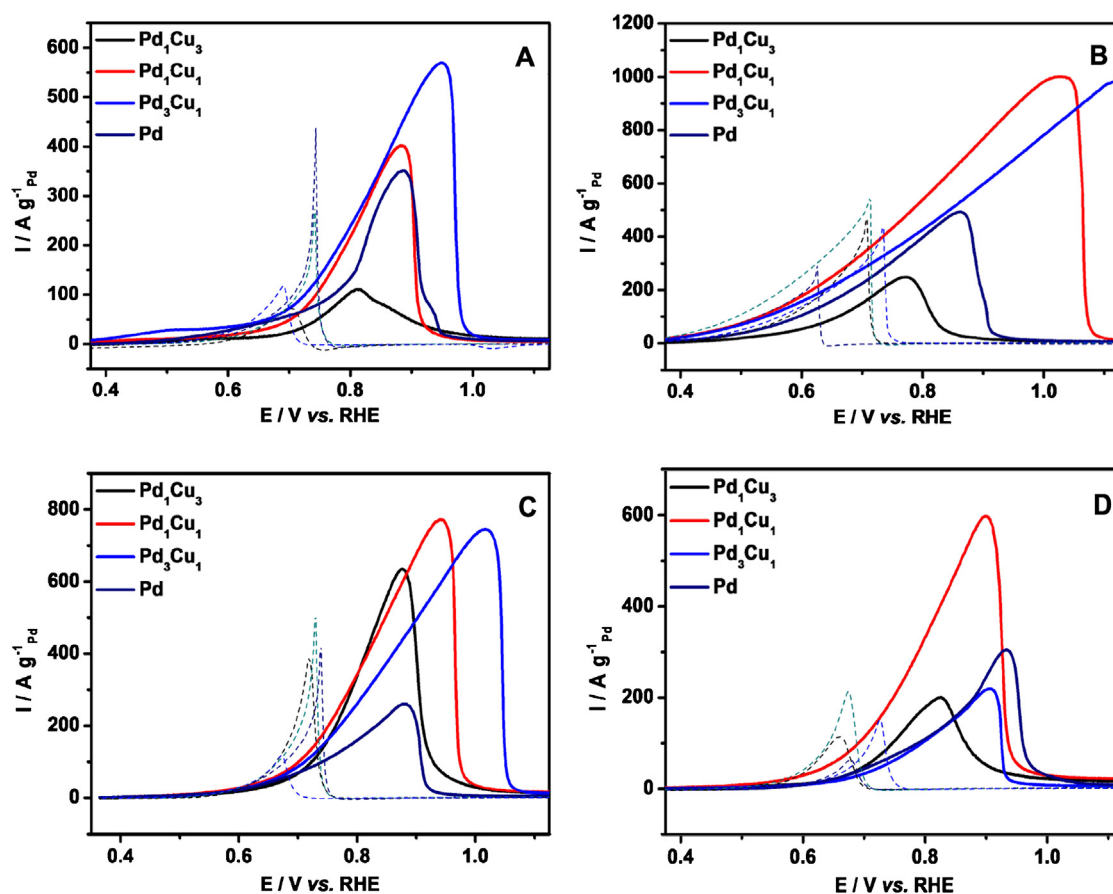
Fig. 4. Cyclic voltammograms of alcohols electrooxidation by Pd_xCu_y catalysts: (A) MeOH, (B) EtOH, (C) ethylene glycol and (D) glycerol. $PdCu_3$ (black), PdCu (red), Pd_3Cu (blue) and Pd (navy). Conditions: 1 M KOH + 1 M MeOH/EtOH (0.1 M EG/glycerol), catalyst loading $-200\,\mu g\,cm^{-2}$, $\Omega = 1600$ revolutions per minute, $\nu = 0.020\,V\,s^{-1}$. Forward scan: full lines, backward scan: dotted lines. (For interpretation of the references to colour in this figure legend, the reader is referred to the web version of this article.)

observed for Pd_3Cu and Pd for the EG oxidation reaction (EGOR) and the EOR, whereas the Tafel slopes (for EOR) and onset potentials are similar, which is an indication of similar specific activity of the active sites. This shows that the palladium-copper solid solution must have a higher density of active sites compared to metallic palladium, which is in perfect agreement with a surface chemical composition obtained by XPS. On the other hand, the larger MOR currents measured at low potential values ($0.4 < E < 0.6\,V$ *vs.* RHE) on Pd_xCu_y *vs.* Pd (especially for the Pd_3Cu catalyst, see Fig. 4A) show that the PdCu solid solution exhibits improved MOR kinetics as compared to palladium, which also implies that the above mentioned PdCu solid solution participates in full electrooxidation of methanol. The electrochemical processes in GOR at Pd_3Cu, PdCu and $PdCu_3$ have characteristics of a kinetic rate determining step (associated with adsorption of alcohol molecule), which was shown by the linear behavior of their activity between 0.4 and 0.8 V *vs.* RHE: $b = 140–185\,mV\,dec^{-1}$. This result indicates that the Pd_xCu_y solid solution has no influence on the intrinsic reaction kinetics in the case of GOR. The slight improvement in onset potentials (Table 1) observed for the oxidation of methanol and glycerol (for at least one composition), implies that the addition of copper to palladium leads to modifications in chemisorption properties, which is usually associated with adsorption of oxygenated molecules on the surface of electrocatalysts. Different copper oxides may play a dual role in the electrocatalytic activity of the synthetized palladium-based catalysts. Previously in the literature Xu et al. have demonstrated the promotion effect of CeO_2, NiO, Co_3O_4, and Mn_3O_4 on palladium electrocatalysts with clear improvement of the electrooxidation performance for a number of different alco-

hols [47,48]. Further analysis of the published data revealed that both CuO and Cu_2O compounds possess intrinsic electrocatalytic activity in the reaction of electrooxidation of oxygenated species such as glucose and sucrose [49,50]. It was also reported that addition of CuO to the platinum catalysts increases the overall activity in the reactions of methanol electrooxidation [51]. The promotion effect is explained by the increased surface coverage of the catalytic materials with OH^- groups which participated in the reaction. On the other hand, it should be taken into consideration that Cu_2O and CuO are poor electrical conductive materials, and by increasing their concentration the overall conductivity will be decreased. In the case of electrocatalysis this will lead to the decrease in measured current densities. In addition, copper oxides may influence mechanistic pathway of alcohols electrooxidation, which can be co-catalyzed by Cu_2O and CuO. As it was shown in Ref. [52] there is an optimal ratio between main catalyst (platinum) and oxide co-catalyst (CuO) at which the synergistic effect occurs. Based on the XRD results described in the present article optimal concentration of oxides should be at the level of 30 wt.% for the majority of studied fuels (MOR, EOR, EGOR and GOR). The detailed study of the Cu_2O/CuO hybrids with palladium should be performed and presented in the stand-alone article.

Density Functional Theory (DFT) was used to gain better insight into the system at the atomistic level. The DFT calculations performed at present study were based on the Perdew-Burke-Ernzerhof (PBE) functional [53,54], and specifically aimed to explore the adsorption of ethanol, methanol, ethylene glycol, glycerol, and OH species on Pd(111) and Pd_3Cu(111) surfaces. Fig. 5 demonstrates that all alcohols interact very weakly with both
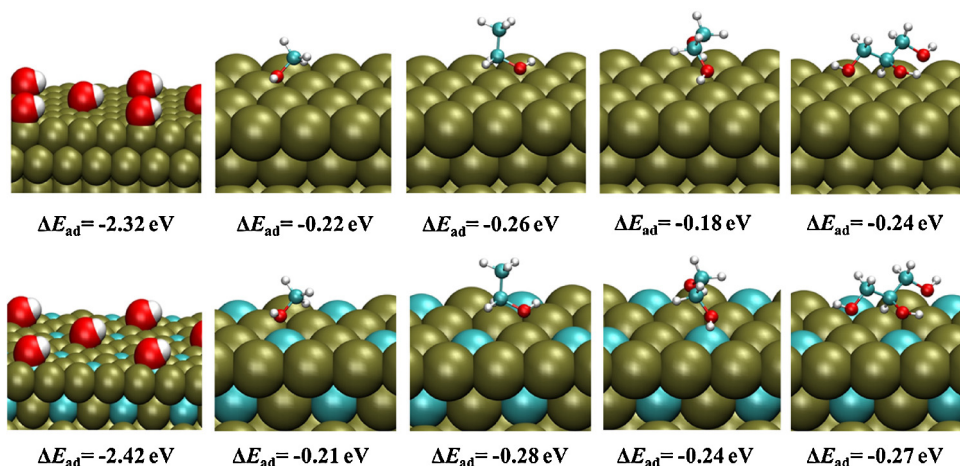
Fig. 5. Optimized structures of hydroxyl, methanol, ethanol, ethylene glycol, and glycerol adsorbed on Pd(111) and Pd$_3$Cu(111) surfaces as calculated using Density Functional Theory with the Perdew-Burke-Ernzerhof (PBE) functional [53,54] and Vienna Ab initio Software Package (VASP) [55–58].

selected surfaces, however slightly with higher affinity to the Pd$_3$Cu(111) compared the Pd(111) surface in the case of ethanol, ethylene glycol, and glycerol.

The adsorption energies of methanol, ethanol, ethylene glycol, and glycerol were calculated as: −0.22, −0.26, −0.18 and −0.24 eV on the Pd(111) surface and −0.21, −0.28, −0.24 and −0.27 eV on the Pd$_3$Cu(111) surface, respectively. Considering entropy losses associated with the adsorption from water solution, the adsorption of any alcohol would be thermodynamically unfavorable as the small change in electronic energy associated with the adsorption will not compensate for the loss of entropy. However, the samples synthesized using the SSM are highly nanostructured. Therefore, due to the confinement of the reactive species in the material pores, entropic losses associated with the adsorption are much smaller, which decreases the adsorption potential of the alcohols. Summing up, the SSM method improves the apparent catalytic activity, not just by increasing the total electrochemically active surface area (as proposed from the electrochemical experiments), but also by decreasing the Gibbs free energy for the adsorption of the considered reactants. This effect is especially important for the adsorption of reactants that interact with the catalytic surface by weak dispersion forces, such as interactions of the herein-considered alcohols with Pd and Pd$_3$Cu. OH species chemisorb on the surface of Pd and Pd$_3$Cu and the adsorption energy of OH groups was calculated as −2.32 eV on top of Pd atoms of the Pd(111) surface, −2.31 eV on top of Pd atoms of the Pd$_3$Cu(111) surface and −2.42 eV on top of Cu atoms of the Pd$_3$Cu(111) surface. This results indicates that the surface Cu atoms are more prone to OH-adsorption than the Pd surface atoms and confirms the assumption of the promotion effect by copper add-atoms on the palladium catalysts discussed above. If we assume that all the other contributions to the Gibbs free energy of adsorption will not differ significantly on these two surfaces, the calculated adsorption energies show that the adsorption potential of OH on Pd$_3$Cu(111) surface shall be 100 mV smaller than on the Pd(111) surface. The presence of OH species on the surface of the Pd$_3$Cu catalyst at lower cell potentials (at least at the surface Cu atoms) should be beneficial for the overall mechanisms of alcohol oxidation since those species are involved in various steps of the reactions. Thus, their energetically enhanced adsorption and presence in adequate proportion shall be favorable to the turnover frequency of the catalytic sites. These results can also explain the lower activity of PdCu$_3$ for the alcohols oxidation as compared to Pd (for ethanol and methanol oxidation reaction), PdCu and Pd$_3$Cu. Higher concentrations of Cu atoms on the catalysts surface will favor large OH$_{ads}$ coverage at lower cell potentials,

which will decrease the number of metal sites available to adsorb and then electrochemically catalyze (ionize) the alcohols.

Further insights into the reaction mechanisms were obtained by Fourier-transform infra-red (FTIR) spectroscopy. To correlate the spectroscopic and electrochemical results, the electrochemical measurements performed during the acquisition of the FTIR spectra in Fig. 6, are presented in Fig. S3. The difference between the voltamperograms in Fig. S3 and those in Fig. 4 can be explained by the difference in the potential sweep rates used in the two cases: $v = 0.001 \, V\,s^{-1}$ in the quasi-stationary conditions of Fig. S3, vs. $v = 0.020 \, V\,s^{-1}$ in Fig. 4. These differences highlight that alcohol and OH$_{ads}$ adsorptions are not only limited by thermodynamics but also by kinetics phenomena. The first steps of alcohol oxidation, i.e. the alcohol adsorption on the catalyst surface occur at ca. $E = 0.09 - 0.4 \, V$ vs. RHE, as shown by the appearance of bands at 1010–1070 cm^{-1}, which can be attributed to the various adsorbed alcohols. The oxidation itself occurs at higher potentials, ca. 0.6 V vs. RHE for the EOR, as revealed by the presence of CO$_2$ (total oxidation−2340 cm^{-1}) and acetaldehyde/acetate (partial oxidation − 1700 cm^{-1}). It should be noted that acetate species are in solution at higher potentials, i.e. $E = 0.65 \, V$ vs. RHE, as shown by the band at 1280 cm^{-1} [59–64]. The first steps of MOR occur at lower potentials, with total oxidation observed above $E = 0.68 \, V$ vs. RHE, which is in agreement with the kinetics analysis discussed above.

According to Simoes [64] and Zalineeva [15], the band at 1070–1100 cm^{-1} indicates the presence of glyceraldehyde, the formation of which is required to produce the glycerate ion [10]. The appearance of oxalate, an intermediate species involved in the EGOR [65,66], was observed at 0.57 V vs. RHE. Total oxidation and C—C bond cleavage occur on all catalysts, as demonstrated by the CO$_2$ band appearance at 2340 cm^{-1} at $E = 0.60 \, V$ vs. RHE for the EOR, GOR and EGOR and $E = 0.65 \, V$ vs. RHE for the MOR (Fig. 6 and Fig. S3). However, partial oxidation still occurs for EOR, as shown by the continued presence of the band at 1280 cm^{-1}, ascribed to "in-solution" acetate (Table 2).

Chronoamperometry experiments were carried out using the Pd$_3$Cu electrocatalyst and different alcohols (Fig. 7) to study the catalysts susceptibility toward surface poisoning. This electrocatalyst was selected as one of the best for alcohols electrooxidation reactions, and being the material in which copper-added active sites were associated with FCC PdCu phase only. It can be clearly seen that the stability of the experimental curve for the GOR was remarkable. On the other side, all other alcohols exhibit a non-negligible current decrease in the timeframe of the experiment, which is indicative of the catalyst poisoning by intermediate species.
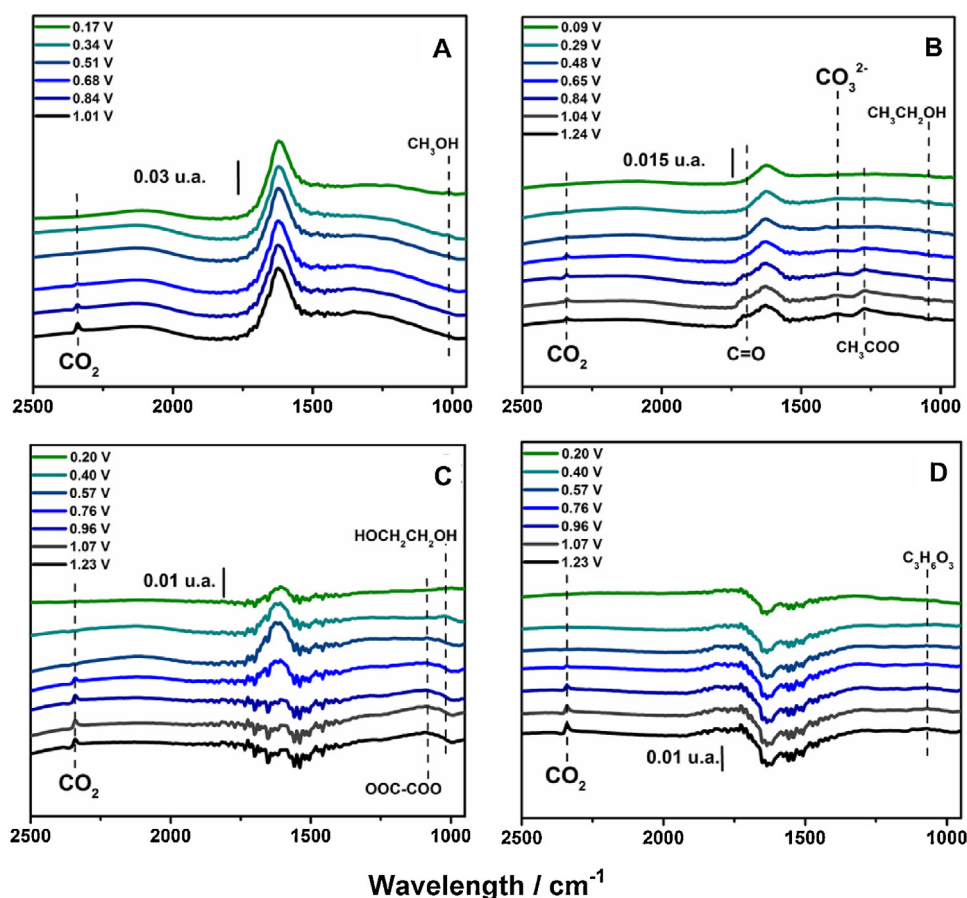
Fig. 6. *In situ* IRRAS spectra of alcohol electrooxidation on Pd$_3$Cu: (A) MeOH, (B) EtOH, (C) EG and (D) glycerol. Conditions: 0.1 M KOH +1 M MeOH/EtOH (0.1 M EG/glycerol), potential values expressed in V *vs.* RHE.

Table 2
Band identification of chemical species by wavenumber and potential of their detection (V *vs.* RHE) for intermediates of different alcohol oxidized *in situ* on Pd$_x$Cu$_y$.

	Species	Wavelength (cm^{-1})	Potentials (V vs. RHE)
Methanol	CO$_2$	2340	0.68
	CH$_3$OH	1000–1020	0.15–0.85
Ethanol	CO$_2$	2340	0.6
	C=O (acetaldehyde, acetate)	1700	0.65
	CO$_3^{2-}$ (in C—H plane)	1360–1380	0.84
	CH$_3$COO$_{sol}$	1270–1280	0.65
	CH$_3$COOH	1040	0.09–0.84
Ethylene Glycol	CO$_2$	2340	0.6
	OOC—COO$_{ads}$	1060–1080	0.57
	HOCH$_2$CH$_2$OH	1020	0.2–0.57
Glycerol	CO$_2$	2340	0.6
	C$_3$H$_6$O$_3$	1070	0.4

Differential Electrochemical Mass Spectrometry (DEMS) measurements were carried out at the PdCu catalyst with a 1 mM L^{-1} ethylene glycol as a fuel in 0.1 M L^{-1} KOH solution using the experimental procedures described above.

The CO$_2$ current efficiency (CCE, i.e. the proportion of the oxidation current corresponding to the production of CO$_2$, calculated as in Ref. [67]) for the ethylene glycol oxidation at the PdCu electrocatalyst was quantified by differential electrochemical mass spectrometry (DEMS), based on the calibration of the $m/z = 22$ and $m/z = 44$ signals using CO-stripping voltammetry (Fig. S4). As obtained results were compared to DEMS data measured with Acta® 3020 anode catalyst as industrial reference for a supported Pd catalyst. Under potentiostatic conditions, CCE around 40% were found in the potential range of 0.6 < E < 0.7 V *vs.* RHE for the PdCu electrocatalyst (Fig. 8). In comparison, the CCE for the commercial

Acta® catalyst in the same potential window stayed below 10%, which demonstrates that Cu adjunction is not only efficient in promoting larger alcohol oxidation currents, but also enables to direct the EGOR towards a complete pathway. Similar onset potentials for the PdCu electrocatalysts of about $E = 0.6$ V *vs.* RHE were found in the MSCV (Fig. S4) and FTIR (Fig. S3) spectra. The onset potential in DEMS is identical for both the $m/z = 22$ (signature of CO$_2^{++}$, attributed solely to CO$_2$ in the present conditions) and $m/z = 44$ (signature of CO$_2^+$ or of a C$_2$H$_4$O$^+$ fragment of any aldehydes). As no increase of the $m/z = 15$ signal is observed, we can conclude that the $m/z = 44$ signal most likely is associated with CO$_2$ evolution. The balance of the faradaic current involved the formation of non-volatile species such as oxalate, that cannot be detected in DEMS but were observed in FTIR, *e.g.* from the O—C—O bands at 1070–1080 cm^{-1} (Fig. 6 and Table 2). Finally, the lack of $m/z = 15$ signal close to the
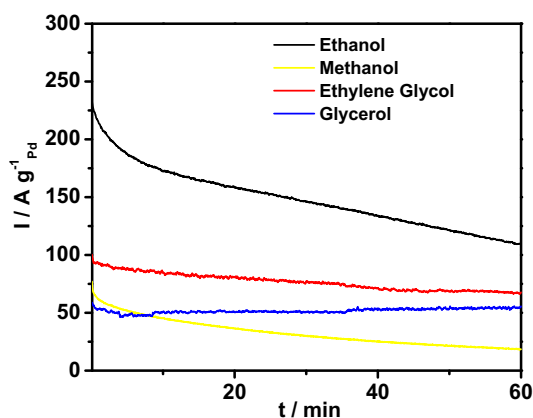
Fig. 7. Chronoamperograms plotted to the Pd_3Cu electrocatalyst at $E = 0.7$ V *vs.* RHE for 0.1 M glycerol, 0.1 M ethylene glycol, 1 M ethanol and 1 M methanol. Conditions: 1 M KOH, RT, no rotation, N_2 purge.
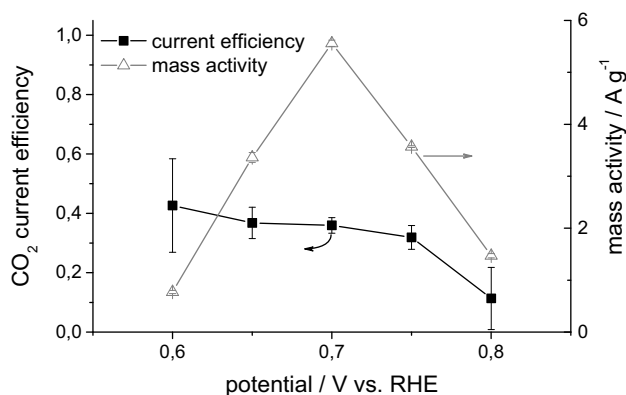

Fig. 8. DEMS results for the ethylene glycol oxidation at the PdCu electrocatalyst in 0.1 M KOH solution containing 1 mM EG: CCE under potentiostatic conditions values recorded after $t = 20$ min.

hydrogen evolution region rules out any methane formation, as formerly found for palladium [68] or platinum-based electrocatalyst [69,70].

Based on this study we can conclude that the addition of add-atoms can increase a catalytic activity of palladium for electrooxidation of oxygenated fuels. Several crucial points have to be considered when designing a new palladium based material: (i) second element should be hydrophilic; (ii) second element or its compounds should not interfere with electronic conductivity of final material; (iii) in the case of easy susceptibility to oxidation, the oxide phase of add-atoms should work as a co-catalyst and should not prevent the access of fuel to active sites and removal the products from the active sites; and (iv) add-atom should affect the mechanism of fuel oxidation (to CO_2 if the final goal is creation of fuel cell device or to Value Added Products if the goal is to make an electrochemical reactors), and vi) detailed mechanism should be evaluated by in situ experimental methods (DEMS, FTIR etc).

4. Conclusions

A series of Pd_xCu_y electrocatalysts was synthesized by the modified SSM and characterized by SEM, TEM, BET and XRD. It was found that the SSM enables preparation of highly dispersed non-supported materials with high surface area. TEM micrographs and XRD diagrams revealed that the electrocatalysts nanoparticles were finely dispersed into small crystallites organized in larger agglomerates, with no significant coalescence within the agglomerates,

except for the $PdCu_3$ samples. The presence of copper in adjunction of palladium promotes methanol, ethanol, ethylene glycol and glycerol electrooxidation, especially in the cases of the PdCu and Pd_3Cu electrocatalysts, resulting in decreased onset potentials and larger oxidation currents. This positive effect was related to the presence of surface copper sites, which favor OH_{ads} species adsorption, which was confirmed by the use of DFT calculations. An unusual increase of the activity in the electrooxidation of ethylene glycol was also observed for $PdCu_3$ catalyst, which can be attributed to the presence of metallic copper and Cu_2O. The decreased palladium content is an attractive economic feature for industrial applications of these catalysts. Based on the results of in situ FTIR experiments the C-C bond cleavage was demonstrated for all the Pd_xCu_y electrocatalysts. Based on the observed results and their analysis we suggested strategies for the rational design of Pd-X materials. We believe that after their further optimization, all studied Pd-Cu electrocatalysts may be used in combined reactors for electricity and value-added products manufacturing.

Appendix A. Supplementary data

Supplementary data associated with this article can be found, in the online version, at http://dx.doi.org/10.1016/j.apcatb.2016.03.016.

References

[1] W. Vielstich, A. Lamm, H.A. Gasteiger, Handbook of Fuel Cells, Wiley, Chichester, 2003.
[2] H.A. Gasteiger, W. Vielstich, H. Yokokawa, Handbook of Fuel Cells, John Wiley & Sons Ltd., Chichester, 2009.
[3] S. Wasmus, A.J. Kuver, Electroanal. Chem. 461 (1999) 14.
[4] E. Antolini, Energy Environ. Sci. 2 (2009) 915–931.
[5] A. Serov, T. Nedoseykina, O. Shvachko, C.J. Kwak, Power Sources 195 (2010) 175–180.
[6] A. Serov, C. Kwak, Catal. Commun. 10 (2009) 1551–1554.
[7] S. Song, P. Tsiakaras, Appl. Catal. B 63 (2006) 187–193.
[8] A. Serov, C. Kwak, Appl. Catal. B 97 (2010) 1–12.
[9] X. Yu, P.G. Pickup, J. Power Sources 182 (2008) 124–132.
[10] A. Serov, C. Kwak, Appl. Catal. B 98 (2010) 1–9.
[11] A. Serov, C. Kwak, Appl. Catal. B 91 (2009) 1–10.
[12] U.B. Demirci, P. Miele, Energy Environ. Sci. 2 (2009) 627–637.
[13] U. Tylus, Q. Jia, K. Strickland, N. Ramaswamy, A. Serov, P. Atanassov, S. Mukerjee, J. Phys. Chem. C 118 (2014) 8999–9008.
[14] A. Serov, K. Artyushkova, P. Atanassov, Adv. Energy Mater. (2014), http://dx.doi.org/10.1002/aenm.201301735.
[15] A. Zalineeva, A. Serov, M. Padilla, U. Martinez, K. Artyushkova, S. Baranton, C. Coutanceau, P.J. Atanassov, Am. Chem. Soc. 136 (2014) 3937–3945.
[16] A. Serov, U. Tylus, K. Artyushkova, S. Mukerjee, P. Atanassov, Appl. Catal. B Environ. 150 (2014) 179–186.
[17] A. Serov, A. Aziznia, P.H. Benhangi, K. Artyushkova, P. Atanassov, E. Gyenge, J. Mater. Chem. A 1 (2013) 14384–14391.
[18] A. Serov, U. Martinez, P. Atanassov, Electrochem. Commun. 34 (2013) 185–188.
[19] A. Serov, M.H. Robson, M. Smolnik, P. Atanassov, Electrochim. Acta 109 (2013) 433–439.
[20] M.H. Robson, A. Serov, K. Artyushkova, P. Atanassov, Electrochim. Acta 90 (2013) 656–665.

[21] S. Brocato, A. Serov, P. Atanassov, Electrochim. Acta 87 (2013) 361–365.
[22] A. Serov, M.H. Robson, K. Artyushkova, P. Atanassov, Appl. Catal. B 127 (2012) 300–306.
[23] A. Serov, M.H. Robson, M. Smolnik, P. Atanassov, Electrochim. Acta 80 (2012) 213–218.
[24] A. Serov, U. Martinez, A. Falase, P. Atanassov, Electrochem. Commun. 22 (2012) 193–196.
[25] A. Serov, M.H. Robson, B. Halevi, K. Artyushkova, P. Atanassov, Electrochem. Commun. 22 (2012) 53–56.
[26] A. Falase, M. Main, K. Garcia, A. Serov, C. Lau, P. Atanassov, Electrochim. Acta 66 (2011) 295–301.
[27] D.A. Konopka, M. Li, K. Artyushkova, N. Marinkovic, K. Sasaki, R. Adzic, T.L. Ward, P. Atanassov, J. Phys. Chem. C 115 (2011) 3043–3056.
[28] P.W. Faguy, N.S. Marinkovic, Appl. Spectrosc. 50 (1996) 394–400.
[29] S. Hu, L. Scudiero, S. Ha, Electrochim. Acta 83 (2012) 354–358.
[30] U.W. Hamm, et al., Electrochim. Acta 43 (1998) 2969–2978.
[31] R. Parsons, T. VanderNoot, J. Electroanal. Chem. 257 (1988) 9–45.
[32] F. Ines, L.-C. Jiang, P. Derek, J. Electrochem. Soc. 130 (1983) 2187–2192.
[33] X.H. Xia, T. Iwasita, J. Electrochem. Soc. 140 (1993) 2559–2565.
[34] M. Watanabe, M. Horiuchi, S. Motoo, J. Electroanal. Chem. 250 (1988) 117–125.
[35] R.R. Adzic et al, J. Electroanal. Chem. 80 (1977) 81–99.
[36] R.R. Adzic, et al., J. Electroanal. Chem. 65 (Part 2) (1975) 587–601.
[37] C. Bianchini, P.K. Shen, Chem. Rev. 109 (2009) 4183–4206.
[38] A. Marchionni, et al., ChemSusChem 6 (2013) 518–528.
[39] S. Motoo, M. Watanabe, J. Electroanal. Chem. 69 (1976) 429–431.
[40] M. Watanabe, S. Motoo, J. Electroanal. Chem. 60 (1975) 259–266.
[41] R.M. Modibedi, T. Masombuka, M.K. Mathe, Int. J. Hydrogen Energy 36 (2011) 4664–4672.
[42] W. Du, K.E. Mackenzie, D.F. Milano, N.A. Deskins, D. Su, X. Teng, ACS Catal. 2 (2012) 287–297.
[43] E.E. Switzer, T.S. Olson, A.K. Datye, P. Atanassov, M.R. Hibbs, C.J. Cornelius, Electrochim. Acta 54 (2009) 989–995.
[44] Z. Zhang, L. Xin, K. Sun, W. Li, Int. J. Hydrogen Energy 36 (2011) 12686–12697.
[45] T. Maiyalagan, K. Scott, J. Power Sources 195 (2010) 5246–5251.
[46] A. Sadiki, P. Vo, S. Hu, T.S. Copenhaver, L. Scudiero, S. Ha, J.L. Haan, Electrochim. Acta 139 (2014) 302–307.
[47] W. Xu, S. Zhu, Z. Li, Z. Cui, X. Yang, J. Power Sources 274 (2015) 1034–1042.
[48] C. Xu, Z. Tian, P. Shen, S.P. Jiang, Electrochim. Acta 53 (2008) 2610–2618.
[49] L. Zhang, H. Li, Y. Ni, J. Li, K. Liao, G. Zhao, Electrochem. Commun. 11 (2009) 812–815.
[50] S. Dong, S. Zhang, X. Cheng, P. He, Q. Wang, Y. Fang, J. Chromatogr. A 1161 (2007) 327–333.
[51] Y. Zhang, Y. Liu, L. Su, Z. Zhang, D. Huo, C. Hou, Y. Lei, Sens. Actuators B 191 (2014) 86–93.
[52] R.S. Amin, R.M. Abdel Hameed, K.M. El-Khatib, H. El-Abd, E.R. Souaya, Int. J. Hydrogen Energy 37 (2012) 18870–18881.
[53] J.P. Perdew, K. Burke, M. Ernzerhof, Phys. Rev. Lett. 77 (1996) 3865.
[54] J.P. Perdew, K. Burke, M. Ernzerhof, Phys. Rev. Lett. 78 (1997) 1396.
[55] G. Kresse, Hafner, J. Phys. Rev. B 47 (1993) 558.
[56] G. Kresse, Hafner, J. Phys. Rev. B 49 (1994) 14251.
[57] G. Kresse, Furthmüller, J. Comput. Mat. Sci. 6 (1996) 15.
[58] G. Kresse, Furthmüller, J. Phys. Rev. B 54 (1996) 11169.
[59] M.H. Shao, R.R. Adzic, Electrochim. Acta 50 (2005) 2415.
[60] F.H.B. Lima, E.R. Gonzalez, Electrochim. Acta 53 (2009) 2963.
[61] A. Kowal, M. Li, M. Shao, K. Sasaki, M.B. Vukmirovic, J. Zhang, N.S. Marinkovic, P. Liu, A.I. Frenkel, R.R. Adzic, N Mater. (2009) 2359.
[62] M. Li, A. Kowal, K. Sasaki, N. Marinkovic, D. Su, E. Korach, P. Liu, R.R. Adzic, Electrochim. Acta 55 (2010) 4331.
[63] M. Li, W.-P. Zhou, N.S. Marinkovic, K. Sasaki, R.R. Adzic, Electrochim. Acta 104 (2013) 454.
[64] M. Simoes, S. Baranton, C. Coutanceau, Appl. Catal. B Environ. 93 (2010) 354.
[65] L. Xin, Z. Zhang, J. Qi, D. Chadderdon, W. Li, Appl. Catal. B Environ. 125 (2012) 85.
[66] L. Wang, H. Meng, P.K. Shen, C. Bianchini, F. Vizza, Z. Wei, Phys. Chem. Chem. Phys. 12 (2011) 2667.
[67] A.B. Delpeuch, T. Asset, M. Chatenet, C. Cremers, J. Electrochem. Soc. 161 (2014) F918.
[68] D.A. Cantane, F.H.B. Lima, Electrocatal 3 (2012) 324.
[69] A. Bach Delpeuch, M. Chatenet, C. Cremers, T. Tübke, Electrochim. Acta 141 (2014) 102.
[70] D. Bayer, C. Cremers, H. Baltruschat, J. Tübke, ECS Trans. 41 (1) (2011) 1669.